Title

Airborne sound propagation over sea during offshore wind farm piling

Running title

Airborne piling noise propagation

Authors

T. Van Renterghem[1], D. Botteldooren, L. Dekoninck

Ghent University, Department of Information Technology, Sint Pietersnieuwstraat 41, B- 9000

Gent, Belgium.

[1] Author to whom correspondence should be addressed. Electronic mail: timothy.van.renterghem@intec.ugent.be

ABSTRACT

Offshore piling for wind farm construction has attracted a lot of attention in recent years due to the extremely high noise emission levels associated with such operations. While underwater noise levels were shown to be harmful for the marine biology, the propagation of airborne piling noise over sea has not been studied in detail before. In this study, detailed numerical calculations have been performed with the Green's Function Parabolic Equation (GFPE) method to estimate noise levels up to a distance of 10 km. Measured noise emission levels during piling of pinpiles for a jacket-foundation wind turbine were assessed and used together with combinations of the sea surface state and idealized vertical sound speed profiles (downwind sound propagation). Effective impedances were found and used to represent non-flat sea surfaces at low-wind sea states 2, 3, and 4. Calculations show that scattering by a rough sea surface, which decreases sound pressure levels, exceeds refractive effects, which increase sound pressure levels under downwind conditions. This suggests that the presence of wind, even when blowing downwind to potential receivers, is beneficial to increase the attenuation of piling sound over the sea. A fully flat sea surface therefore represents a worst-case scenario.

PACS numbers: 43.28.Fp, 43.50.Vt, 43.28.En, 43.28.Js

I. INTRODUCTION

Offshore wind farms are being constructed all over the world at a very high rate. This is not surprising since over sea there is a beneficial combination of a large and constant wind energy potential and space. Such conditions are not always met over land. In between 2000 and 2009 there was an average annual growth of 50 % in offshore wind energy production in the European Union as summarized in Ref. 1. In Ref. 2, The European Wind Energy Association estimates offshore wind energy to take a share of near 40 % in the total EU wind energy production by 2030.

The noise impact of offshore piling during wind farm construction has attracted a lot of attention in recent years, due to the extremely high noise emission levels associated with such operations. Marine piling is one of the techniques typically used in relatively shallow water, and involves a hydraulic hammer driving a pile into the sea-bed. Other common techniques are the use of floating foundations in deep sea or gravity based seabed foundations.

Most scientific studies focus on the underwater impact of such piling activities. Vibrations of impacted poles lead to high immission levels in the water column and sound pulses reach very long distances[3]. Numerical models have been developed and measurements have been performed to assess underwater noise levels during piling[4-8]. Injury and behavioral changes in marine animals have been reported, even at large distances from the piling location[9-12]. To mitigate such impairments, the use of an air bubble curtain has recently shown to be an efficient noise reducing measure during piling[13].

The current study focuses on airborne sound propagation from piling activities. Similarly to underwater sound generation, the noise emission levels above the sea surface are extremely high. In addition, there are specific propagation effects that might lead to high sound pressure levels, even at long distances. Firstly, a flat water surface behaves as a rigid plane for sound reflecting on it. In absence of meteorological effects, pressure doubling is therefore expected at low sound frequencies and at large distances, leading to a 6 dB increase in sound pressure level relative to free field sound propagation conditions. In case of sound propagation over land, in contrast, the interaction with natural and porous soils can reduce sound levels significantly due to the so-called ground effect[14]. Secondly, downwind propagation leads to downward refraction of sound, further increasing sound pressure levels. The combination of a rigid surface and downward refraction could lead to multiple-bounce effects[15] and consequently increased sound pressure levels.

However, windy periods will be accompanied by a rough sea surface. Wind-induced sea surface waves will have a noise mitigation effect and will counteract downward refraction. Coupled analysis of sea state and wind conditions is therefore needed for adequate predictions and to assess the relative importance of both processes.

The effect of a rough sea surface on sound propagation has been studied for both underwater sound[16-19] and airborne sound. Approaches for the latter are discussed in more detail in this paragraph. Sonic boom propagation predictions were shown to be affected by the sea surface state, leading to a decrease in peak overpressure and a rounding of sonic boom wave profiles[20]. Effective impedances were derived for rigid surfaces shaped as semi-cylindrical bosses, wedges

and intersecting parabolas. Based on numerical calculations, Salomons[21] proposed an engineering model for wave scattering in case of a surface profile constructed by a chain of circle segments. Bolin et al.[22] used a ground surface impedance model with adapted parameters to fit his observations of long-distance low-frequency tone (80 Hz and 200 Hz) propagation over sea.

A main goal of this research is to estimate the relevant propagation distances for airborne piling noise, and whether this aspect should be taken into account in future environmental impact assessments. In addition, better knowledge of the propagation effects mentioned before could lead to a selection of suitable meteorological conditions for piling activities if problems are to be expected with noise reaching the coastline.

This study combines sound measurements during offshore piling to use realistic source emission spectra, and detailed numerical propagation calculations under different low-wind sea conditions. The paper is organized as follows. First, the measurement of a piling emission spectrum is described. In a next section, the sound propagation model is discussed briefly, with emphasis on the derivation of effective impedance spectra for low-wind sea surfaces, and coupled to idealized sound speed profiles in the marine atmospheric boundary layer. In a next section, numerical results for sound propagation up to 10 km are presented in presence and absence of a refracting atmosphere. Finally, conclusions are drawn.

II. SOURCE POWER ESTIMATION DURING PILING

Noise measurements to allow estimating the airborne source power spectrum were performed on board of a floating Zodiac, positioned at about 280 m from the piling location. The case

studied concerns a jacket foundation, involving the piling of four steel pinpiles per jacket, to carry a 6.15 MW-wind turbine. The driving of a single pinpile was monitored. The pile has a diameter of 1.829 m and a length of 48 m and was driven in the Thornton sand bank, at about 28 km off the Belgium North Sea coast (C-power project, phase 2-3). The water depth in the area varies approximately from 12 m to 24 m. More details on the constructional aspects of this specific piling operation can be found in Ref. 8.

The pinpiles were driven from a jack-up platform equipped with a re-useable piling template. After the pile was positioned correctly, a soft start procedure was initiated, where the hammer operated at about 20 % of its maximum impact power. In a next phase, the full hammer energy was used. During this phase, about 7 minutes of undisturbed measurements could be made, representing the period of maximum airborne noise emission.

The measurements were performed with a ½" electret microphone (type MK 250 B, Microtech Gefell) with a sensitivity of 44 mV/Pa, connected to a pre-amplifier (type SV 12, Svantek). The microphone capsule has a flat frequency response over the full audible frequency range, and deviations are less than 1 dB up to 15 kHz for normal incident sound. The saturation level exceeds 140 dB (at 1 kHz). The logging of the measurements was done with a Svantek 959 handheld device. The measurement chain was certified as class 1 equipment. The measurement chain was calibrated with a 94-dB class-1 acoustic calibrator (type SV 30 A, Svantek), producing a pure tone at a sound frequency of 1 kHz. A professional weather proof outdoor unit (WME 950, Microtech Gefell) was used, including a wind screen to limit wind-induced microphone noise. Piling was performed under calm wind conditions.

The hammer performed about 48 impacts per minute during that phase. The airborne impact peaks were anticipated by an underwater generated shockwave radiating from the Zodiac floor, reaching the microphone membrane.

In a simple approximation, source power levels are estimated, by calculating back from the measured sound pressure level spectrum to the hammer impact spot at the piling platform, accounting for geometrical divergence (assuming a point source), atmospheric absorption according to ISO9613-1 (see Ref. 23), and a reflection on a (flat) rigid plane, using the ISO9613-2 (see Ref. 24) ground reflection term. The height of the impact spot during piling was estimated at 15 m. Reflections from the body of the person holding the sound level meter, reflections on the surfaces of the boat, or scattering by a non-flat sea surface were not considered here.

Figure 1 shows the equivalent source power level spectrum in between the end of the soft start procedure and the moment when the impact location becomes submersed. In addition, the peak level spectrum, defined as the level exceeded only 1 % of the time (based on the total A-weighted level) during this same period, is depicted.

During piling, the impact location shifts from above water to below water. Impacts under the sea surface also generate airborne noise, however, leading to a drop in level of at least 10 dBA (not shown). Although piling typically lasts longer than could be measured in this specific case, all relevant acoustical power is captured in this time frame. The total A-weighted spectra have their maxima at the 1/3 octave band of 1 kHz, while the total A-weighted peak level is near 145 dBA. Both the equivalent source power level Lw_{eq} and the Lw_1 level will be considered when assessing sound pressure levels in case of long-distance sound propagation over the sea.

[FIGURE 1]

III. MODELING APPROACH

The 2D axisymmetric Green's Function Parabolic Equation (GFPE)[25-26] method has been used for the long-distance propagation calculations over the sea surface. GFPE, like any PE method, simulates one-way sound propagation and this assumption strongly decreases the computational cost. The effective sound speed profile approach allows taking into account vertical gradients in both air temperature and (horizontal) wind speed. In addition, reflection on finite-impedance planes can be accounted for. A major advantage of the GFPE method is that using large steps in the propagation direction does not reduce accuracy, thus enabling calculations up to a distance of 10 km at sufficiently high sound frequencies (in the current study up to 5 kHz). The limiting factor is rather the inhomogeneity of the propagation medium than the sound wave length. During the calculations, stepping is performed at 10 times the wavelength, with a maximum step size of 10 m. The vertical discretisation, on the other hand, is much more demanding and 10 computational cells per wavelength were used.

Including the effect of a non-flat surface in the parabolic equation method can be achieved in various ways. The conformal mapping method[15] approaches the terrain profile by a chain of circle segments, where convex and concave curvatures are transformed to an equivalent upward or downward refracting sound speed profile. The General Terrain PE (GTPE) is applicable to arbitrary terrain profiles and is based on a coordinate transform. It produces accurate results as long as local slopes do not exceed 30°. The rotated reference frame GFPE (rGFPE) is a very efficient method to include terrain undulations[27-28], and has been validated

e.g. for sound propagation in a valley-slope configuration in a mountainous region[28]. However, restrictions on the local slopes do not make this method suitable for representing sea surfaces. In the current study, the effective impedance approach will be used. Ref. 14 discusses that reflection on a rigid rough surface can be approximated by replacing this surface by an equivalent flat finite-impedance plane. This approach is computationally highly efficient.

The GFPE was shown to be accurate for the specific case of sound propagation over the sea surface, and was able to capture the variations in transmission loss due to changing meteorological conditions in between a controlled monochromatic source at sea and a receiver at 10 km near the coast[22].

The airborne sound emitted by impacting on the cylindrical pole is approached as a point source at the average height above the sea surface during the piling operation, which was taken to be 15 m. Starting fields and top absorbing boundary conditions, as described in detail in Ref. 15, were used. The height of the PE grid, excluding the absorbing layer at the top, is chosen to be at least 400 m. This height was shown to be sufficient as taking a larger grid height did not change the final results (namely the predicted total A-weighted piling noise level) at all distances considered. As clipping to the next power of 2 has been performed to efficiently use the fast Fourier transforms on which the GFPE implementation is based, the actual height depends on sound frequency.

Numerical results are summarized per 1/3-octave bands, and 10 sound frequencies were used to constitute each band.

IV. REFRACTION IN THE MARINE BOUNDARY LAYER

The Monin-Obukhov similarity theory (MOST)[29-30], previously shown to be applicable above seas[31], has been used to estimate the vertical temperature and wind speed profiles in the marine atmospheric boundary layer:

$$u_z = \frac{u_*}{\kappa}\left[\ln\left(\frac{z}{z_0}\right) - \Psi_m\left(\frac{z}{L_{MO}}\right)\right], \quad (1)$$

$$\theta_z = \theta_s + \frac{T_*}{\kappa}\left[\ln\left(\frac{z}{z_0}\right) - \Psi_h\left(\frac{z}{L_{MO}}\right)\right], \quad (2)$$

where u_z is the wind speed at height z above the sea surface, κ is the Von Karman constant (=0.4, see e.g. Ref. 32), u_* is the friction velocity, z_0 is the aerodynamic roughness length, L_{MO} is the Monin-Obukhov length, θ_z is the potential air temperature at height z, T_* is the temperature scale, and θ_s is the air temperature at sea level.

In an unstable atmosphere, the functions Ψ_m and Ψ_h can be parameterized as follows:[33]

$$\Psi_m = 2\ln\left(\frac{1+x}{2}\right) + \ln\left(\frac{1+x^2}{2}\right) - 2\tan^{-1}(x) + \frac{\pi}{2}, \quad (3)$$

$$\Psi_h = 2\ln\left(\frac{1+x^2}{2}\right), \quad (4)$$

with

$$x = \left(1 - \gamma_1 \frac{z}{L_{MO}}\right)^{\frac{1}{4}} \text{ and } \gamma_1 = 16 \text{ (see Ref. 33).} \quad (5)$$

In a stable atmosphere, following parameterization can be used[34]:

$$\Psi_m = \Psi_h = -\gamma_2 \frac{z}{L_{MO}}, \tag{6}$$

with γ_2=5 (see Ref. 34).

In a neutral atmosphere, Ψ_m and Ψ_h are both zero. As a result, purely logarithmical wind speed and temperature profiles are then obtained.

The aerodynamic roughness length z_0 is a key parameter, and determines the strength of the gradients near the surface that are essential for refraction of sound waves when emitted at low heights above the sea surface. Charnock[35] related the sea surface aerodynamic roughness length to the friction velocity by the following relation:

$$z_0 = z_{ch} \frac{u_*^2}{g}, \tag{7}$$

where g is the gravitational acceleration (=9.80665 m/s^2) and z_{ch} is commonly referred to as the "Charnock parameter". The latter depends on wave age. Experimental studies yielded values of z_{ch} at open sea of typically 0.011 (see Ref. 36) or 0.012 (see Ref. 37), while near coastal regions, a value of 0.018 (see Ref. 39) or 0.0185 (see Refs. 40 and 41) was found to be appropriate. In the current study, an average value of 0.014 has been used. Clearly, z_0 will increase with increasing wind speed, as stronger winds induce sea surface waves with higher amplitudes. Although somewhat counterintuitive, a fixed ratio between the aerodynamic roughness length and the (average) obstacle height over which the wind blows cannot be found, following Lettau[42].

Wind speed profiles will be identified by the wind speed at the standard meteorological height of 10 m (=u_{10m}). The friction velocity u_* can then be calculated by combining Eqs. (1) and (7).

The surface layer temperature scale T_* is linked to u_* and L_{MO}; the definition of the Monin-Obukhov length can be used to calculate T_*, as discussed e.g. in Ref. 43:

$$L_{MO} = \frac{\theta_s u_*^2}{\kappa g T_*} \tag{8}$$

A standard environmental lapse rate Γ_e of $6.5.10^{-3}$ K/m has been used. The reference air temperature near the sea surface θ_s is taken as 288 K (corresponding to a sound speed equal to 340 m/s). Atmospheric stability classifications based on long-term observations at the North Sea in Ref. 37 showed that neutral atmospheric conditions are most commonly encountered, occurring more than 50 % of the time. Based on the measurements and estimations in Ref. 37, an unstable atmosphere in the current study will be characterized by a value L_{MO}=-100 m, while L_{MO}=100 m is used to represent a stable atmosphere. The latter has a rather limited frequency of occurrence[37-38] .

The effective sound speed profile, as used in the GFPE method, is the sum of the (downwind) horizontal wind velocity component in the sound propagation direction and the adiabatic sound speed as influenced by the height-dependent air temperature:

$$c_z = u_z + \sqrt{\frac{c_p}{c_v} R\left(\theta_z - \Gamma_e z\right)}\,, \tag{9}$$

where c_p/c_v is the ratio of the specific heat capacities at constant pressure and constant volume of air (=1.4), and R is the specific gas constant of dry air (= 287 J/kg/K). Dry air has been assumed when expressing the dependency between air temperature and sound speed in Eq.

(9); however, the effect of the presence of water vapor in air on the sound speed was shown to be very limited[15].

Atmospheric absorption of sound depends on relative humidity, air temperature and ambient atmospheric pressure and is calculated by the engineering approach as presented in ISO 9613-1 (see Ref. 23); the atmospheric pressure is chosen to be 1013.25 hPa, and relative humidity at 80 %.

V. SCATTERING BY A ROUGH SEA SURFACE

A. Wind-induced sea surface representation

A common open sea surface wave spectral density representation *F* is given by the following analytical expression proposed by Pierson and Moskowitz (PM)[44]:

$$F(f_{sea}) = \frac{\alpha g^2}{(2\pi)^4 f_{sea}^5} e^{-1.25\left(\frac{f_{sea,m}}{f_{sea}}\right)^4} \tag{10}$$

where α=8.1 10^{-3} is the empirically determined equilibrium range level[45], f_{sea} is the frequency of the sea surface waves, and $f_{sea,m}$ is the peak frequency of the spectrum, which can be approached by

$$f_{sea,m} = 0.13\frac{g}{u_{10m}}. \tag{11}$$

This spectral representation of the sea surface assumes that sea waves are in full equilibrium with the wind. This needs wind blowing steadily during a long period over a large area. The merits of the PM model have been confirmed by Alves and Banner[46], although some slight

modifications were proposed. Since the widespread use of this original model, and its good fits with measured data, the original model is employed in this study. Other models have been proposed for non-fully developed wind waves at sea (like the JONSWAP spectrum[47]), where additional parameters like e.g. the fetch are needed.

Different sea surface realizations were constructed by multiplying the amplitude of the (normalized) Fourier transform of a generated white noise surface with the PM spectral density function. The random phase of the white noise was retained. In a next step, the sea surface is obtained by calculating the inverse spatial Fourier transform. As a result, the relative ratio of energy present at different sea wave frequencies follows the PM model. The absolute amplitudes were calculated based on the following relationship, linking the significant wave height H_s (i.e. the wave height, trough to crest, at the highest third of all waves present at the sea surface) and wind speed[46,48]:

$$H_s = 0.02466 u_{10m}^2 . \quad (12)$$

A correlation coefficient of R=0.99 was reported in Ref. 46 using Eq. (12). The maximum wave height is taken as 2 times the significant wave height, which is consistent with the properties of the applicable Rayleigh spatial distribution for sea wave height[49].

B. Effective impedance of the sea surface

Calculations have been performed for sea states 2, 3, and 4, for which the wind fields are described as a “light”, “gentle” and “moderate” breeze, respectively. Wind speeds at a height of

10 m are then 3 m/s, 5 m/s, and 7 m/s. The significant wave heights, averaged over the 15 realizations for each wind speed, are 0.22 m, 0.53 m, and 1.00 m.

Effective impedances have been derived in a similar way as discussed in detail in Ref. 20. Sound propagation over many realizations of the sea surface is calculated with a full-wave 2D numerical model. The main interest is sound propagation at near-grazing incidence, as the source emission height during piling is low compared to the propagation distances of interest. To limit the computational cost, source and receiver are consequently positioned at limited height above the undulating surface. The source and receiver are separated by 5 m, and were located at 0.5 m above the sea surface which average water surface variation was in all cases zero. The angle of incidence is therefore 0.199 rad (11.42°). In case either the source or receiver would lie below the sea surface because of waves, additional realizations were constructed. To prevent edge effects, a sufficiently large undulating area in front of the source, and also behind the receiver, is included in the sound propagation domain.

The linear 2D finite-difference time-domain (FDTD) method[50] has been used, which is generally recognized as a reference solution in case of such complex sound propagation problems. The undulating sea surfaces are modelled using a uniform Cartesian grid. As a result, synthetic stair-case scattering effects could be expected, the more the surfaces of each cell are modelled as rigid. This is overcome by applying a spatial discretisation of only 1 cm to better follow the undulations of the sea surface, leading to 17 computational cells per wavelength at the maximum sound frequency used in deriving the effective impedances (which is 2 kHz). Such a fine spatial mesh is beyond what is needed for accurate calculations in case of free field sound

propagation to keep the phase error limited[51]. Computational efficiency is enhanced by simulating a broadband acoustic pulse, allowing to find the response over a wide frequency range with a single simulation. In Fig. 2, sound scattering as a result of single realizations of the different sea states are depicted. Following the PM sea surface wave model, with increasing sea state number, there is a shift to (dominant) low-frequency surface waves. Compared to the rigid and flat sea case (sea state 0), scattering of sound is clearly visible, strongly affecting sound waves when reflecting at the sea surface.

In a next step, sound pressure levels, relative to free field sound propagation, of each realization for a given sea state, are linearly averaged to find the "ground effect". As the average height of the sea surface realizations is in all cases zero, there is no need to raise the effective impedance plane to enhance fits as was proposed in Ref. 20.

[FIGURE 2]

Next, the parameters of an analytical expression for the frequency dependent impedance were looked for. An analytical point source model[14] has been used for the latter. The fitting has been performed directly on the sound pressure level data expressed to free field propagation. To increase physical soundness of these fittings, some a-priori conditions have been imposed, namely a decrease of the (relative) impedance Z with increasing sound frequency, real and imaginary parts that are positive, and an absolute value of the relative impedance (which means the absolute impedance of the surface divided by the impedance of air) larger than 1. The form of the curve has been kept deliberately simple, partly inspired on the work reported in Refs. 20 and 22:

$$Z = \frac{a_r}{f^{m_r}} + b_r + \left(\frac{a_j}{f^{m_j}} + b_j \right) j \,, \tag{13}$$

where j is the imaginary unit and a_r, b_r, a_j, b_j, m_r, and m_j are model parameters to be fitted.

The fits to the relative sound pressure levels, and the corresponding impedance curves, are depicted in Figs. 3 and 4, respectively. An overview of the parameter values to be used in Eq. 13 for different sea states is given in Table 1.

[FIGURE 3]

[FIGURE 4]

[TABLE 1]

Note that higher sea states were not considered as a piling operation is typically conducted at calm sea for reasons of safety. In addition, deriving an effective impedance is likely to be unsuccessful when the surface undulation is too high relative to the sound frequencies of interest[20]. Agreement at sound frequencies above roughly 1 kHz becomes already difficult at sea state 4 as illustrated in Fig. 3. Below 1 kHz at sea state 4, and for frequencies up to 2 kHz in the other cases, reasonably good agreement is found giving confidence in the followed engineering approach. There was no interest in approaching the peaky behavior of these scattering curves as this is caused by the random nature of the problem. The effective impedance approach assumes that during sound propagation the sea surface is static.

VI. CALCULATION OF SOUND PRESSURE LEVELS

Sound pressure levels are calculated using following engineering formula:

$$L_p = L_w - 10\log_{10}\left(4\pi r^2\right) - A_{abs} + L_{p,ff} \quad (14)$$

L_w is the airborne source power level by the piling, r is the length of the straight line connecting source and receiver position, A_{abs} is the atmospheric absorption, and $L_{p,ff}$ is the sound pressure level, relative to free field propagation, as calculated with the axi-symmetric GFPE method. The latter includes refraction effects, and rough sea surface reflection and scattering.

VII. NUMERICAL RESULTS

A. Flat sea-surface in absence of wind

Numerical calculations in absence of wind are presented in Fig. 5. In addition, calculation results are provided employing a standardized engineering model for outdoor sound propagation namely ISO9613-2 (see Ref. 24). Refraction of sound is not included in this model, and reflection on a non-porous plane (so fully rigid, factor G=0 as proposed in Ref. 24) has been used. This model shows to neglect some of the interferences at distances smaller than 1 km from the source, but gives a very similar prediction as GFPE at larger distances. The Lw_1 spectrum is somewhat stronger peaked at 1 kHz than Lw_{eq}. As a result, the difference in predicted level between the equivalent level and the peak level at long distance is smaller than at close distance due to atmospheric absorption.

[FIGURE 5]

B. Rough sea-surface including downwind effects

Fig. 6 shows that the sea surface undulations in combination with their accompanying wind profiles (downwind sound propagation) generally lead to lower sound pressure levels than in case of a still and perfectly flat sea surface. However, in specific zones at close distance (less than 600 m from the source) total A-weighted levels from piling could be similar or even slightly enhanced relative to sound propagation in absence of wind.

[FIGURE 6]

The sound speed profiles under downwind conditions increase sound pressure levels relative to the absence of wind, while the undulating sea surface decreases levels relative to a fully flat one. Sea surface scattering is the most important effect, especially when the atmosphere is neutral or unstable. In case of a stable atmosphere, sea surface scattering is still more important, however, somewhat less pronounced compared to neutral or unstable conditions. In case there is wind, the different low-wind sea states give rather similar sound pressure levels. A systematic increase or decrease in level with increasing sea state is not predicted in the range of distances considered.

When only accounting for refraction (over a flat and rigid sea surface, so deliberately neglecting rough sea surface scattering typical for a given wind speed), an increase in level of 8-10 dBA is calculated at 10 km relative to sea state 0 (no refraction and perfectly flat sea surface) as depicted in Fig. 7. When analyzing the sea surface scattering effect separately (see Fig. 8), deliberately neglecting refraction of sound, the differences between sea states 2, 3 and 4 are very small within 2 km from the source. At larger distances, these differences rapidly increase. At 10 km, the sea surface representative for sea state 4 would potentially lead to a decrease in

level of 10 dBA relative to sea state 3, and to more than 15 dBA relative to sea state 2. Atmospheric absorption was included in the simulations that decouple refraction and sea surface state. However, as discussed before, combined analysis of sea state and wind profile is needed to come to realistic predictions.

[FIGURE 7]

[FIGURE 8]

As an example, the predicted sound pressure level spectra at various distances in case of sea state 3, under neutral conditions, are depicted in Fig. 9. These calculations clearly show that the piling noise becomes very low frequent after long distance propagation, as both atmospheric absorption and sea surface wave scattering strongly attenuates the high frequency part of spectrum. Up to about 2 km, the 1 kHz 1/3-octave band dominates the spectrum.

[FIGURE 9]

VIII. CONCLUSIONS

Long-distance propagation over sea of (measured) airborne noise emission from piling of pinpiles for jacket-foundation offshore-wind turbines was numerically studied. Simplified effective impedance spectra, representative for sea states 2, 3 and 4, were derived in the current study. Full-wave calculations over various realizations of wind-induced undulating sea surfaces, corresponding to the Pierson and Moskowitz surface wave spectral density relation, were used as starting point. The effective impedance curves were then used in the GFPE method to account for sea surface scattering, in combination with refraction of sound by

vertical sound speed profiles in the marine atmospheric boundary layer. The current numerical analysis stresses the need to apply prevailing combinations of vertical refraction profiles and sea surface states, especially at large distances from the piling location.

The sea surface scattering effect exceeds the downwind refraction effect when assessing the attenuation of piling sound with distance. A flat sea surface in absence of refraction is most favorable for long-distance sound propagation of piling noise, leading to maximum sound pressure levels. Up to a few kilometers, piling noise is expected to be easily hearable. At distances exceeding 10 km, the noise impact is expected to be very low under the wind conditions considered. However, the predicted difference in equivalent A-weighted total sound pressure level between different (down)wind conditions may amount up to 25 dBA (unstable atmosphere) or 15 dBA (neutral atmosphere) at 10 km from the piling location (see Fig. 6). A stable atmosphere in combination with downwind sound propagation only gives a benefit of near 5 dBA relative to sound propagation over a flat sea surface in absence of refraction as shown in Fig. 6. However, stable conditions occur much less frequently based on long-term meteorological observations.

IX. CONCLUDING REMARKS

The source power levels from piling employed in the current study were measured in a realistic setting. However, they cannot be easily generalized. The emitted noise strongly depends on the size of the hammer, the dimensions of the pole, and the properties of the sea floor. In addition, specific operational choices during piling could have an important influence on the produced airborne noise levels. In the current engineering approach, point source emission was assumed.

Using an equivalent impedance plane to represent a rough sea surface was shown to be a computationally highly efficient approach once its parameters are assessed. While this method can be useful from an engineering point of view, some limitations should be mentioned. Firstly, the variation in acoustic effect at different (random) realizations of a specific sea surface is rather large, increasing uncertainty on the final numerical results. Secondly, replacing sound scattered at the sea surface by (equivalent) absorption does not fully hold in case of downwind sound propagation. Upwardly scattered sound waves can be bent downwards again by wind, potentially still reaching the receiver. However, such contributions are expected to be of limited importance, as such sound paths would typically involve multiple interactions with the rough sea surface, making it unlikely that a specific sound path is successively directed towards the receiver. In addition, the low-wind conditions considered in this study lead to rather limited wind speed gradients near the sea surface. Another limitation of the effective impedance approach is that only the coherent part of the sound field is accounted for. Long-distance propagation over a rigid rough surface might lead to a considerable transfer of sound energy to the incoherent part of the sound field[14].

In the current analysis, focus is on downwind sound propagation as this gives rise to higher sound pressure levels compared to cross-wind or upwind conditions. Turbulence is not included here as downward refraction is typically dominant over atmospheric scattering (see e.g. examples calculated in Ref. 15). The measurements described in Bolin et al.[22] were mainly made during upwind sound propagation conditions. During such episodes, including turbulence scattering was shown to be essential to come to realistic predictions explaining the variability in

level over time. However, levels will be much lower than during downwind propagation and piling noise would most likely fully disappear in the ambient background noise.

The Monin-Obukhov similarity theory has been used to estimate vertical wind speed and temperature profiles in the marine boundary layer. It is expected that the atmospheric height of relevance exceeds the range of validity of this model given the large propagation distance aimed at. Consequently, care is needed when using the results for the largest distances considered. Nevertheless, it can be reasonably expected that above the height of validity such profiles only change slowly, therefore not strongly influencing sound propagation anymore. To overcome this problem, measured vertical profiles would be needed.

In the marine atmospheric boundary layer, also vertical humidity profiles will appear, which could influence sound propagation to some extent. The latter effect has not been accounted for in the current study.

Additional sensitivity analyses showed that the specific choice of the Charnock parameter z_{ch} in the typical range of values observed at open sea and near coastal regions (see Section IV) could lead to a level change of less than 0.4 dBA at 10 km (for sea state 3 and when assuming a stable atmosphere). Also the height of the source, relative to the sea surface, might significantly change due to tides. Additional calculations of source heights set at 10 m and 20 m (compared to 15 m which was used as a default value in the calculations in this paper) showed variations of less than 0.5 dBA at 10 km (for sea state 3 and when assuming a stable atmosphere).

REFERENCES

[1] R. Green and N. Vasilakos, "The economics of offshore wind," Energ. Policy **39**, 496–502 (2011).

[2] European Wind Energy Association, "Pure power: wind energy scenarios up to 2030," report (2008).

[3] P. Madsen, M. Wahlberg, J. Tougaard, K. Lucke, and P. Tyack, "Wind turbine underwater noise and marine mammals: implications of current knowledge and data needs," Mar. Ecol. Prog. Ser. **309**, 279-295 (2006).

[4] C. de Jong and M. Ainslie, "Underwater radiated noise due to the piling for the Q7 offshore wind park," Proceedings of Acoustics '08, Paris, France (2008).

[5] H. Bailey, B. Senior, D. Simmons, J. Rusin, G. Picken, and P. M. Thompson, "Assessing underwater noise levels during pile driving at an offshore windfarm and its potential effects on marine mammals," Mar. Pollut. Bull. **60**, 888–897 (2010).

[6] M. Zampolli, M. Nijhof, C. de Jong, M. Ainslie, E. Jansen, and B. Quesson, "Validation of finite element computations for the quantitative prediction of underwater noise from impact pile driving," J. Acoust. Soc. Am. **133**, 72–81 (2013).

[7] P. Reinhall and P. Dahl, "Underwater Mach wave radiation from impact pile driving: Theory and observation," J. Acoust. Soc. Am. **130**, 1209–1216 (2011).

[8] A. Norro, B. Rumes, S. Degraer, "Differentiating between Underwater Construction Noise of Monopile and Jacket Foundations for Offshore Windmills: A Case Study from the Belgian Part of the North Sea," Sci. World J., 897624 (2013).

[9] J. Tougaard, J. Carstensen, J. Teilmann, H. Skov, and P. Rasmussen, "Pile driving zone of responsiveness extends beyond 20 km for harbour porpoises (*Phocoena phocoena*, (L.))," J. Acoust. Soc. Am. **126**, 11-14 (2009).

[10] J. Tougaard, O. Henriksen, and L. Miller, "Underwater noise from three offshore wind turbines: estimation of impact zones for harbor porpoises and harbor seals," J. Acoust. Soc. Am. **125**, 3766-3773 (2009).

[11] J. David, "Likely sensitivity of bottlenose dolphins to pile driving noise," Water Environ. J. **20**, 48-54 (2006).

[12] J. Carstensen, O. Henriksen, and J. Teilmann, "Impacts on harbour porpoises from offshore wind farm construction: Acoustic monitoring of echolocation activity using porpoise detectors (T-PODs)," Mar. Ecol. Prog. Ser. **321**, 295-308 (2006).

[13] K. Lucke, P. Lepper, M. Blanchet, and U. Siebert, "The use of an air bubble curtain to reduce the received sound levels for harbour purpoises," J. Acoust. Soc. Am. **130**, 3406–3412 (2011).

[14] K. Attenborough, K. Li, K. Horoshenkov, *Predicting outdoor sound* (Taylor and Francis, London and New York, 2007), 456 pages.

[15] E. Salomons, *Computational atmopsheric acoustics* (Kluwer, Dodrecht, 2001), 348 pages.

[16] J. Senne, A. Song, M. Badiey, and K. Smith, "Parabolic equation modeling of high frequency acoustic transmission with an evolving sea surface," J. Acoust. Soc. Am. **132**, 1311–1318 (2012).

[17] S. Walstead and G. Deane, "Reconstructing surface wave profiles from reflected acoustic pulses," J. Acoust. Soc. Am. **133**, 2597–2611 (2013).

[18] C. Eckart, “The scattering of sound from the sea surface,” J. Acoust. Soc. Am. **25**, 566-570 (1953).

[19] S. Mitchell and F. Machell, “Observations of low-frequency acoustic interaction with the ocean surface,” J. Acoust. Soc. Am. **86**, 1118-1123 (1989).

[20] P. Boulanger and K. Attenborough, “Effective impedance spectra for predicting rough sea effects on atmospheric impulsive sounds,” J. Acoust. Soc. Am. **117**, 751-762 (2005).

[21] E. Salomons, “Computational study of sound propagation over undulating water,” Proceedings of 19th International Congress on Acoustics, Madrid, Spain (2007).

[22] K. Bolin, M. Boué, and I. Karasalo, “Long range sound propagation over a sea surface,” J. Acoust. Soc. Am. **126**, 2191-2197 (2009).

[23] ISO 9613-1: “Acoustics - Attenuation of sound during propagation outdoors - Part 1: Calculation of the absorption of sound by the atmosphere,” International Organisation for Standardisation, Geneva, Switzerland (1993).

[24] ISO 9613-2: “Acoustics – attenuation of sound during propagation outdoors - Part 2:General method of calculation,” International Organisation for Standardisation, Geneva, Switzerland (1996).

[25] K. Gilbert and X. Di, “A fast Green’s function method for one-way sound propagation in the atmosphere,” J. Acoust. Soc. Am. **94**, 2343–2352 (1993).

[26] E. Salomons, “Improved Green’s function parabolic equation method for atmospheric sound propagation,” J. Acoust. Soc. Am. **104**, 100–111 (1998).

[27] P. Blanc-Benon and D. Juve, “Outdoor sound propagation in complex environments: Recent developments in the PE method,” Proceedings of Forum Acusticum 2002, Sevilla, Spain (2002).

[28] T. Van Renterghem, D. Botteldooren, and P. Lercher, “Comparison of measurements and predictions of sound propagation in a valley-slope configuration in an inhomogeneous atmosphere," J. Acoust. Soc. Am. **121**, 2522-2533 (2007).

[29] A. Obukhov, “Turbulence in an atmosphere with non-uniform temperature,” Trudy Inst. Teoret. Geofiz. Nauk SSSR **1**, 95–115 (1946). Translation in Bound.-Layer Meteorol. **2**, 7-29 (1971).

[30] A. Monin and A. Obukhov, “Basic laws of turbulent mixing in the surface layer of the atmosphere,” Trudy Geofiz. Inst. Aca. Nauk SSSR **24**, 163–187 (1954).

[31] J. Edson, C. Fairall, “Similarity relationships in the marine atmospheric surface layer for terms in the TKE and scalar variance budgets,” J. Atmos. Sci. **55**, 2311-2328 (1998).

[32] U. Högström, “Review of some basic characteristics of the atmospheric surface layer,” Boundary-Layer Meteorol. **78**, 215–246 (1996).

[33] C. Paulson, “The mathematical representation of wind speed and temperature profiles in the unstable atmospheric surface layer,” J. Appl. Meteorol. **9**, 857-861 (1970).

[34] A. Dyer, “A review of flux-profile relationships,” Bound.-Lay. Meteorol. **7**, 363-372 (1974).

[35] H. Charnock, “Wind stress over a water surface,” Quart. J. Roy. Meteorol. Soc. **81**, 639–640 (1955).

[36] S. Smith, “Coefficients for sea surface wind stress, heat flux and wind profiles as a function of wind speed and temperature,” J. Geophys. Res. **93**, 15467–15474 (1988).

[37] A. Peña and S. Gryning, “Charnock’s Roughness Length Model and Non-dimensional Wind Profiles Over the Sea,” Bound.-Lay. Meteorol. **128**, 191-203 (2008).

[38] A. Van Wijk, A. Beljaars, A. Holtslag, and W. Turkenburg, “Evaluation of stability corrections in wind speed profiles over the North Sea,” J. Wind Eng. Ind. Aerod. **33**, 551-566 (1990).

[39] H. Johnson, J. Højstrup, H. Vested, S. Larsen, “On the Dependence of Sea Surface Roughness on Wind Waves,” J. Phys. Oceanogr. **28**, 1702–1716 (1998).

[40] H. Johnson, “Simple expressions for correcting wind speed data for elevation,” Coast. Eng. **36**, 263–269 (1999).

[41] J. Wu, “Wind-Stress coefficients over Sea surface near Neutral Conditions—A Revisit,” J. Phys. Oceanogr. **10**, 727–740 (1980).

[42] H. Lettau, “Note on Aerodynamic Roughness-Parameter Estimation on the Basis of Roughness-Element Description,” J. Appl. Meteor. **8**, 828-832 (1969).

[43] A. L’Esperance, J. Nicholas, K. Wilson, D. Thomson, Y. Gabillet, and G. Daigle, ‘‘Sound propagation in the atmospheric surface layer: Comparison of experiment with FFP predictions,’’ Appl. Acoust. **40**, 325-346 (1993).

[44] W. Pierson and L. Moskowitz, “A proposed spectral form for fully developed wind seas based on the similarity theory of A. A. Kitaigorodskii,” J. Geophys. Res. **69**, 5181–5190 (1964).

[45] O. Phillips, “The equilibrium range in the spectrum of wind-generated waves,” J. Fluid Mech. **4**, 426-434 (1958).

[46] J. Alves and M. Banner, “Revisiting the Pierson Moskowitz Asymptotic Limits for Fully Developed Wind Waves,” J. Phys. Oceanogr. **33**, 1301-1323 (2003).

[47] D. Hasselmann, M. Dunckel, and J. Ewing, “Directional Wave Spectra Observed during JONSWAP 1973,” J. Phys. Oceanogr. **10**, 1264–1280 (1980).

[48] D. Carter, “Prediction of wave height and period for a constant wind velocity using the JONSWAP results,” Ocean Eng. **9**, 17-33 (1982).

[49] E. Thornton and R. Guza, “Transformation of wave height distribution,” J. Geophys. Res. **88**, 5925-5938 (1983).

[50] D. Botteldooren, “Finite-difference time-domain simulation of low-frequency room acoustic problems,” J. Acoust. Soc. Am. **98**, 3302-3308 (1995).

[51] T. Van Renterghem and D. Botteldooren, “Prediction-step staggered-in-time FDTD: an efficient numerical scheme to solve the linearised equations of fluid dynamics in outdoor sound propagation,” Appl. Acoust. **68**, 201-216 (2007).

TABLES

TABLE I. Overview of best-fitted parameters to be used in Eq. 13 to represent a rough sea surface (for sea states 2, 3 and 4) in the effective impedance plane approach.

	sea state		
fitted parameters	2	3	4
a_r	763000	9260	30000000
b_r	3.00	4.00	2.50
m_r	2.20	1.30	3.50
a_j	30862	80000	3000000
b_j	2.03	2.00	3.00
m_j	1.50	1.90	3.00

FIGURE CAPTIONS

Fig. 1. The estimated source power level spectrum during piling. L_{Weq} is the equivalent source power level, L_{W1} is the source power level exceeded only 1% of the time.

Fig. 2. (Color online) Snapshots of sound pulse propagation in case of a fully flat sea surface (sea state 0) and sea states 2, 3, and 4. These full-wave time-domain calculations illustrate the scattering process for sound emitted at grazing incidence above the sea surface. An arbitrary logarithmical scale has been used.

Fig. 3. Results of the fits on the surface interaction spectra as calculated by the full-wave calculations (FDTD), averaged over 15 realizations, and the best fitted effective impedance plane approach using an analytical point source model. In (a) sea state 2 is considered, in (b) sea state 3, and in (c) sea state 4. The thin lines in each plot indicate the averaged curve plus or minus the standard deviation as obtained from the different realizations.

Fig. 4. (Color online) Relative sea surface impedances in function of sound frequency, for sea states 2, 3 and 4 (indicated as subscripts). The real part of the impedances and the (negative) imaginary part are depicted separately. In case of sea state 0, the relative impedance is purely real and infinite.

Fig. 5. Predicted total sound pressure level with distance in absence of refraction, employing detailed numerical calculations (GFPE) and a standardized engineering model for outdoor sound propagation (ISO9613-2). The immission predictions represented by the full lines start from the equivalent source power level (Lw_{eq}), the dashed lines use the 1% highest source power levels (Lw_1). A fixed receiver height of 2 m above a rigid and perfectly flat sea surface is used, the receptor points used in this plot are spaced at 10 m.

Fig. 6. (Color online) Predicted total (equivalent) sound pressure level with distance as a result from the monitored piling operation for different sea states (combined refraction and sea surface profiles). Sea sate 0 (no refraction, perfectly flat and rigid sea surface) is shown for comparison in each subplot. In (a), a neutral atmosphere is assumed, in (b) a stable atmosphere, and in (c) and unstable atmosphere.

Fig. 7. (Color online) Predicted total (equivalent) sound pressure level with distance as a result from the monitored piling operation for different sea states, deliberately neglecting sea surface scattering (a rigid and flat sea surface is modelled in all cases). Sea sate 0 (no refraction, perfectly flat and rigid sea surface) is shown for comparison in each subplot. In (a), a neutral atmosphere is assumed, in (b) a stable atmosphere, and in (c) and unstable atmosphere.

Fig. 8. (Color online) Predicted total (equivalent) sound pressure level with distance as a result from the monitored piling operation for different sea states, deliberately neglecting refraction (a homogeneous and still atmosphere is modelled in all cases). Sea sate 0 (no refraction, perfectly flat and rigid sea surface) is shown for comparison in each subplot.

Fig. 9. (Color online) Predicted (equivalent) sound pressure level spectra at different distances (500 m, 1 km, 2 km, 5 km and 10 km; receiver height 2 m), relative to the piling location, for sea state 3 (assuming a neutral atmosphere). The measured equivalent source power spectrum Lw_{eq} is shown (dashed black line) as well; the frequency range 50 Hz- 5 kHz (full black line) has been considered for the propagation calculations.

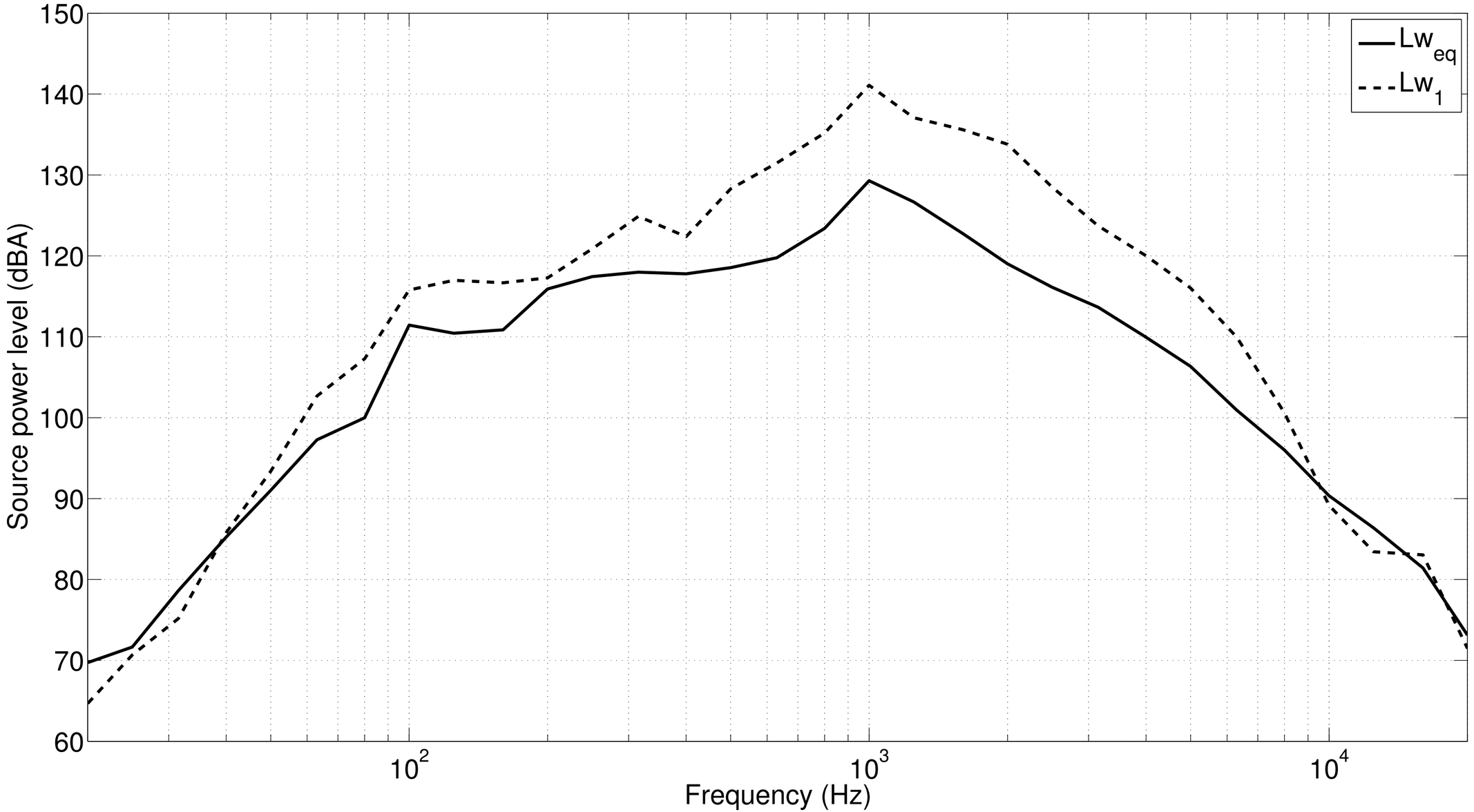
150
140
130
120
110
100
90
80
70
60
Source power level (dBA)
10^2
10^3
10^4
Frequency (Hz)
Lw_{eq}
Lw_1

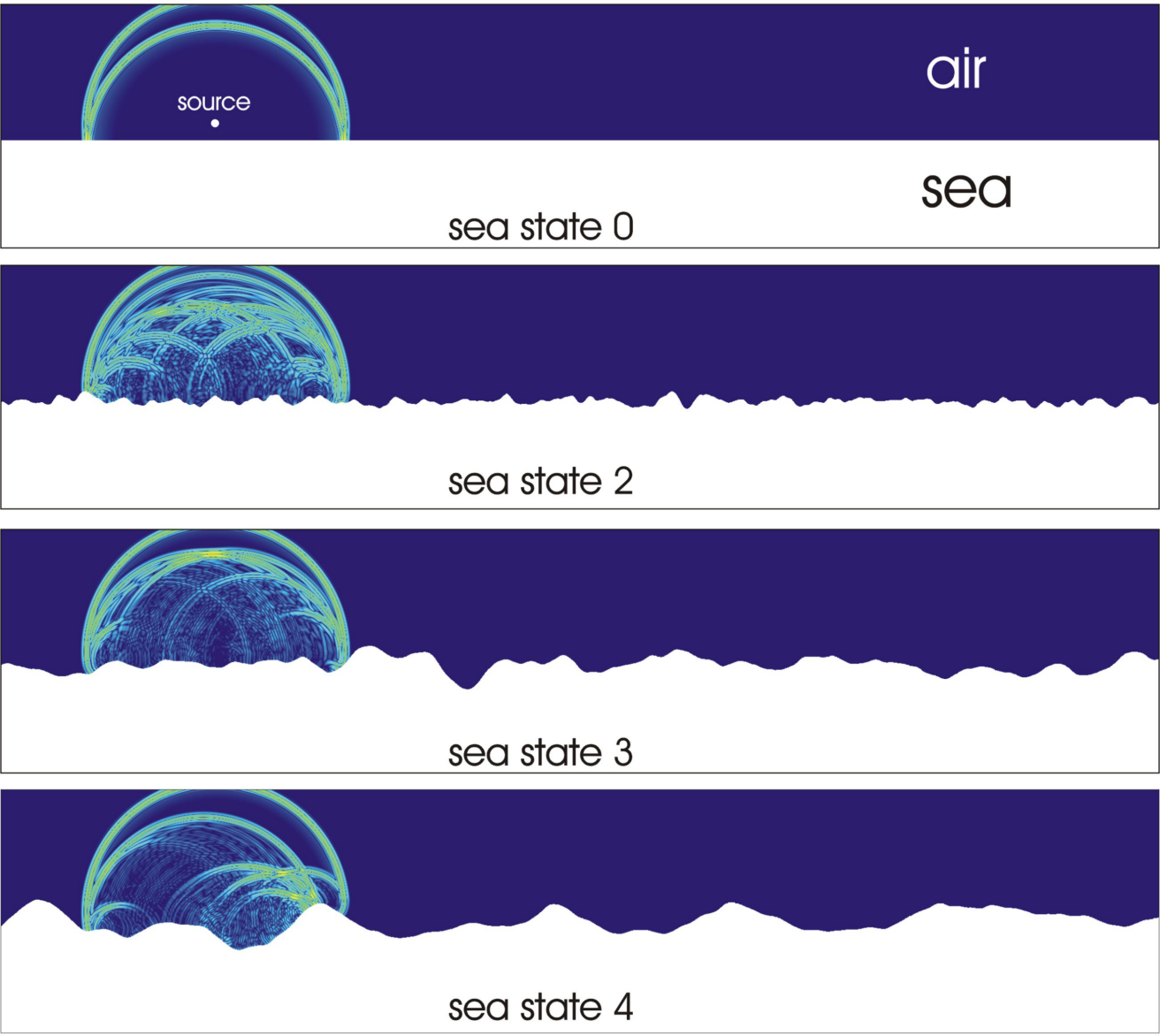
source
air
sea
sea state 0
sea state 2
sea state 3
sea state 4

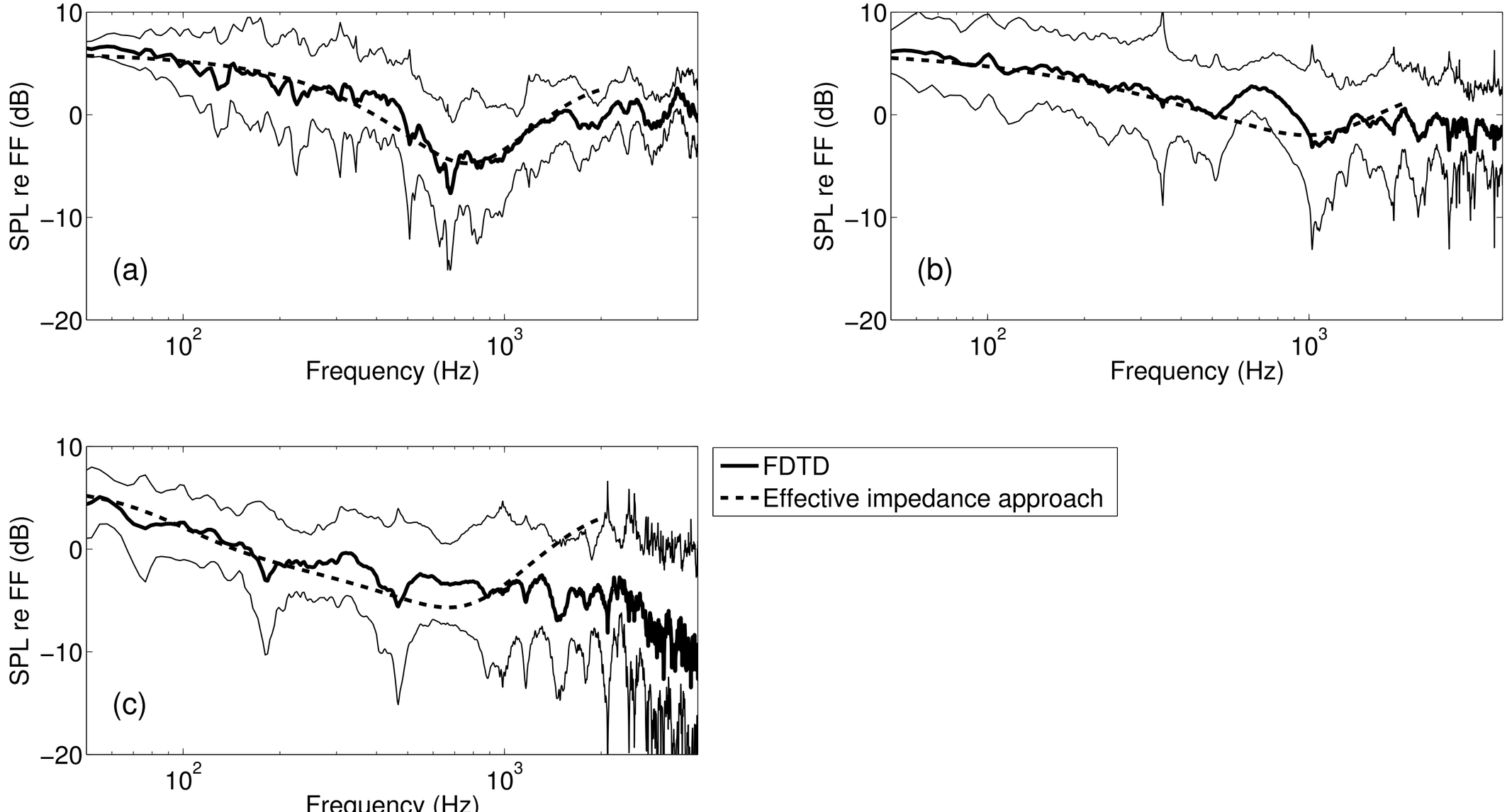
10
0
−10
−20
SPL re FF (dB)
(a)
10^2
10^3
Frequency (Hz)
(b)
(c)
FDTD
Effective impedance approach

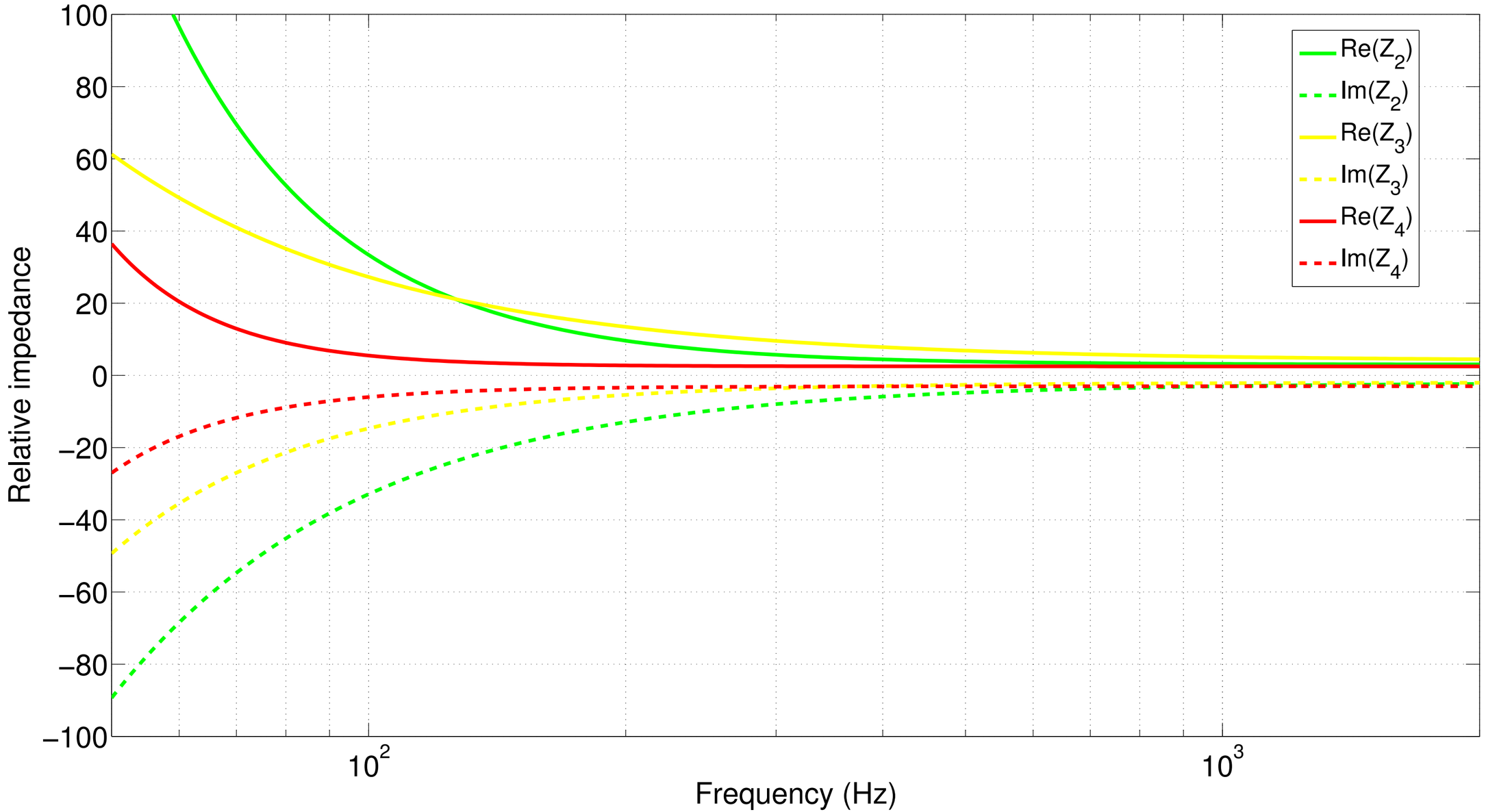
100
80
60
40
20
0
−20
−40
−60
−80
−100
Relative impedance
10^2
10^3
Frequency (Hz)
Re(Z_2)
Im(Z_2)
Re(Z_3)
Im(Z_3)
Re(Z_4)
Im(Z_4)

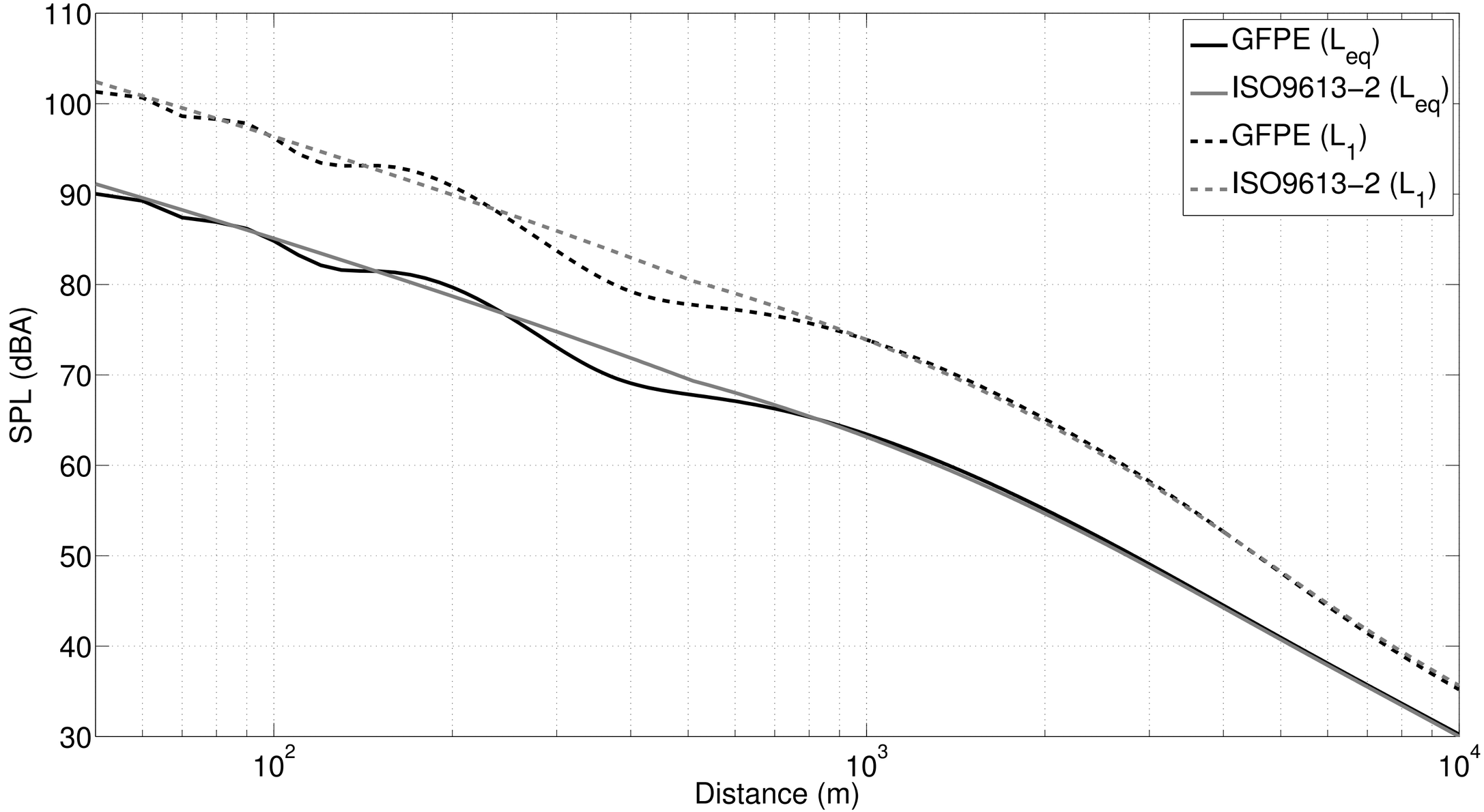
GFPE (L_{eq})
ISO9613–2 (L_{eq})
GFPE (L_1)
ISO9613–2 (L_1)
SPL (dBA)
Distance (m)
110
100
90
80
70
60
50
40
30
10^2
10^3
10^4

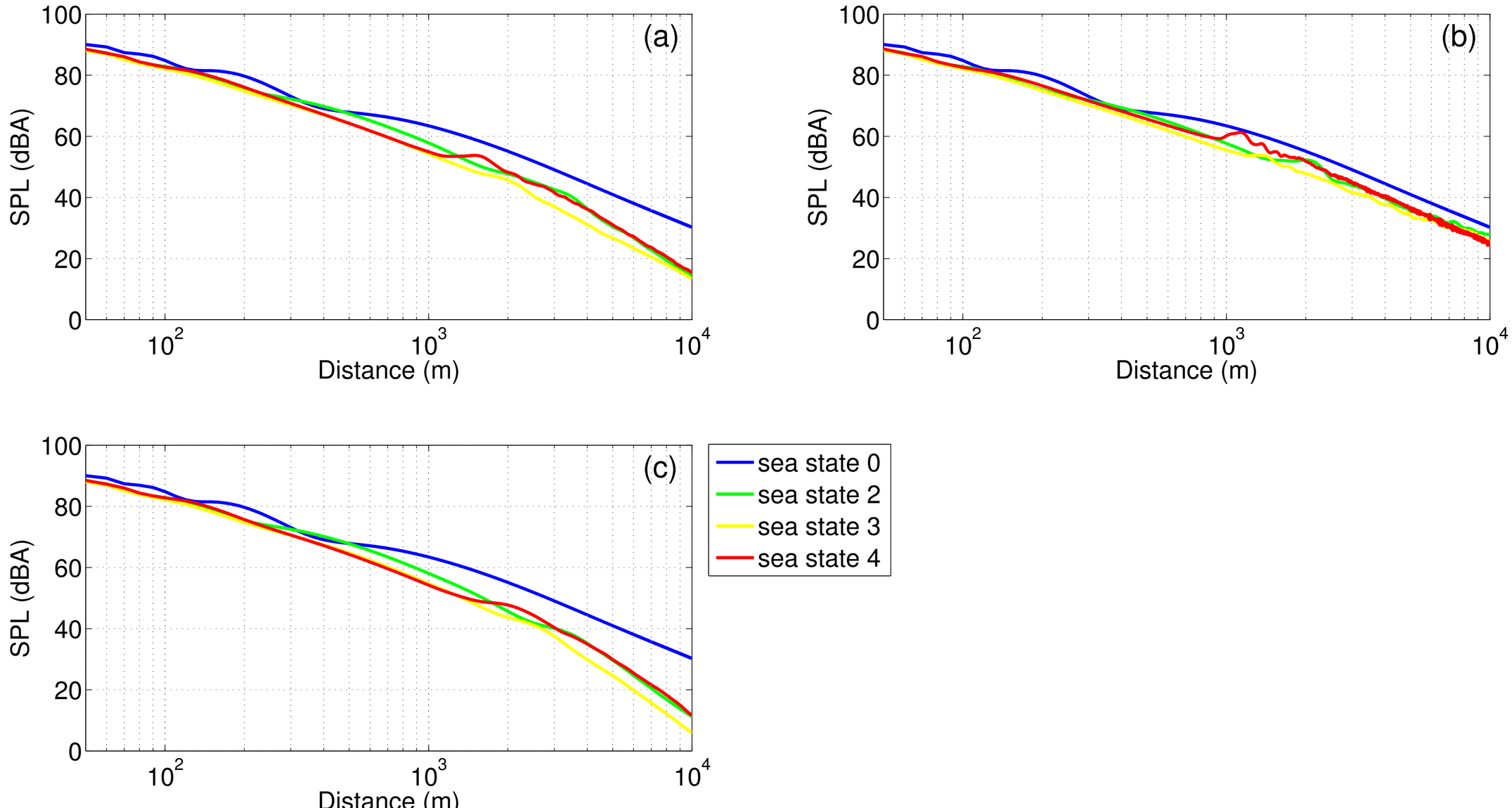
(a)
(b)
(c)
SPL (dBA)
Distance (m)
100
80
60
40
20
0
10^2
10^3
10^4
sea state 0
sea state 2
sea state 3
sea state 4

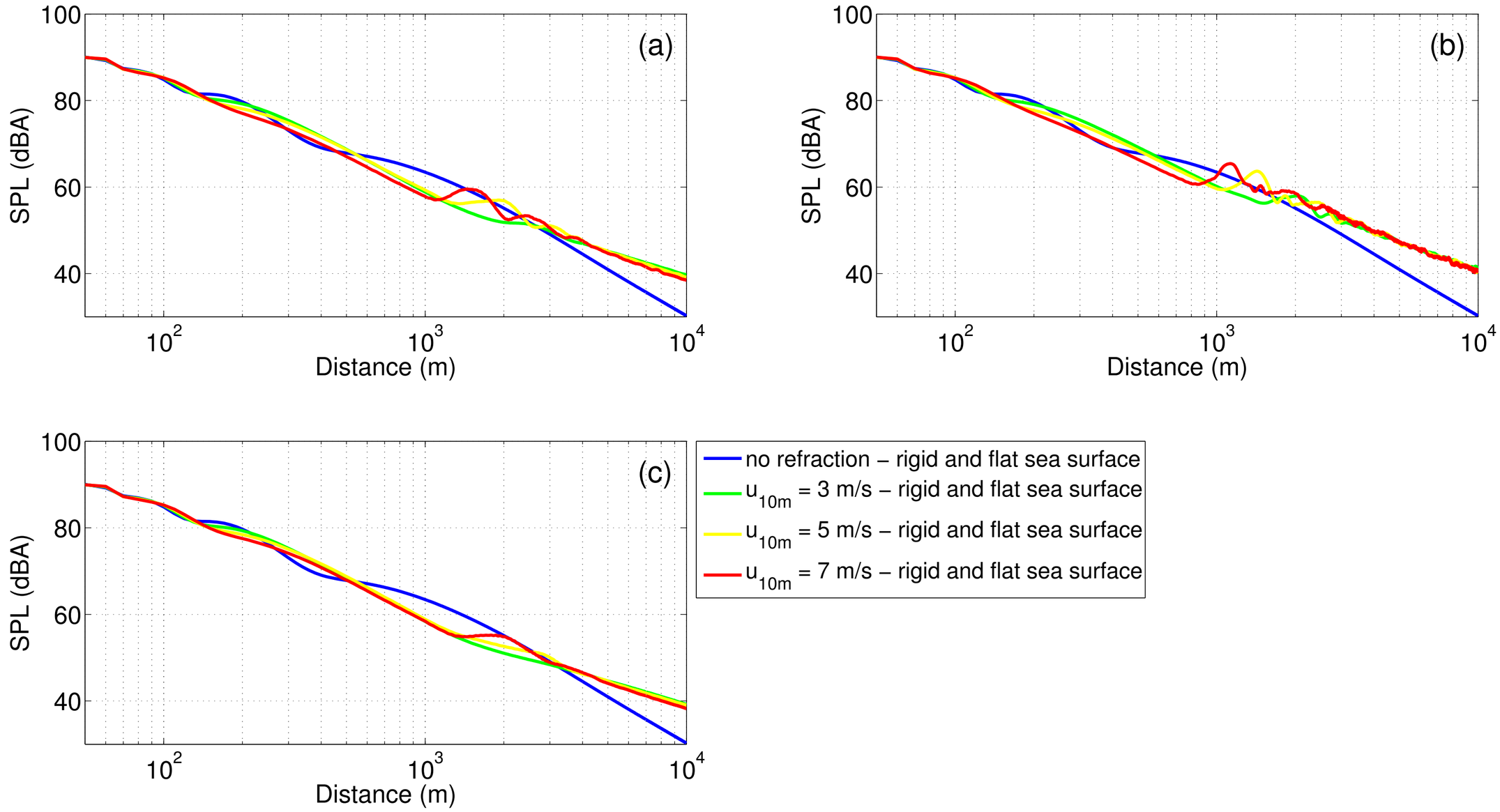
(a)
(b)
(c)
100
80
60
40
SPL (dBA)
10^2
10^3
10^4
Distance (m)
no refraction – rigid and flat sea surface
u_{10m} = 3 m/s – rigid and flat sea surface
u_{10m} = 5 m/s – rigid and flat sea surface
u_{10m} = 7 m/s – rigid and flat sea surface

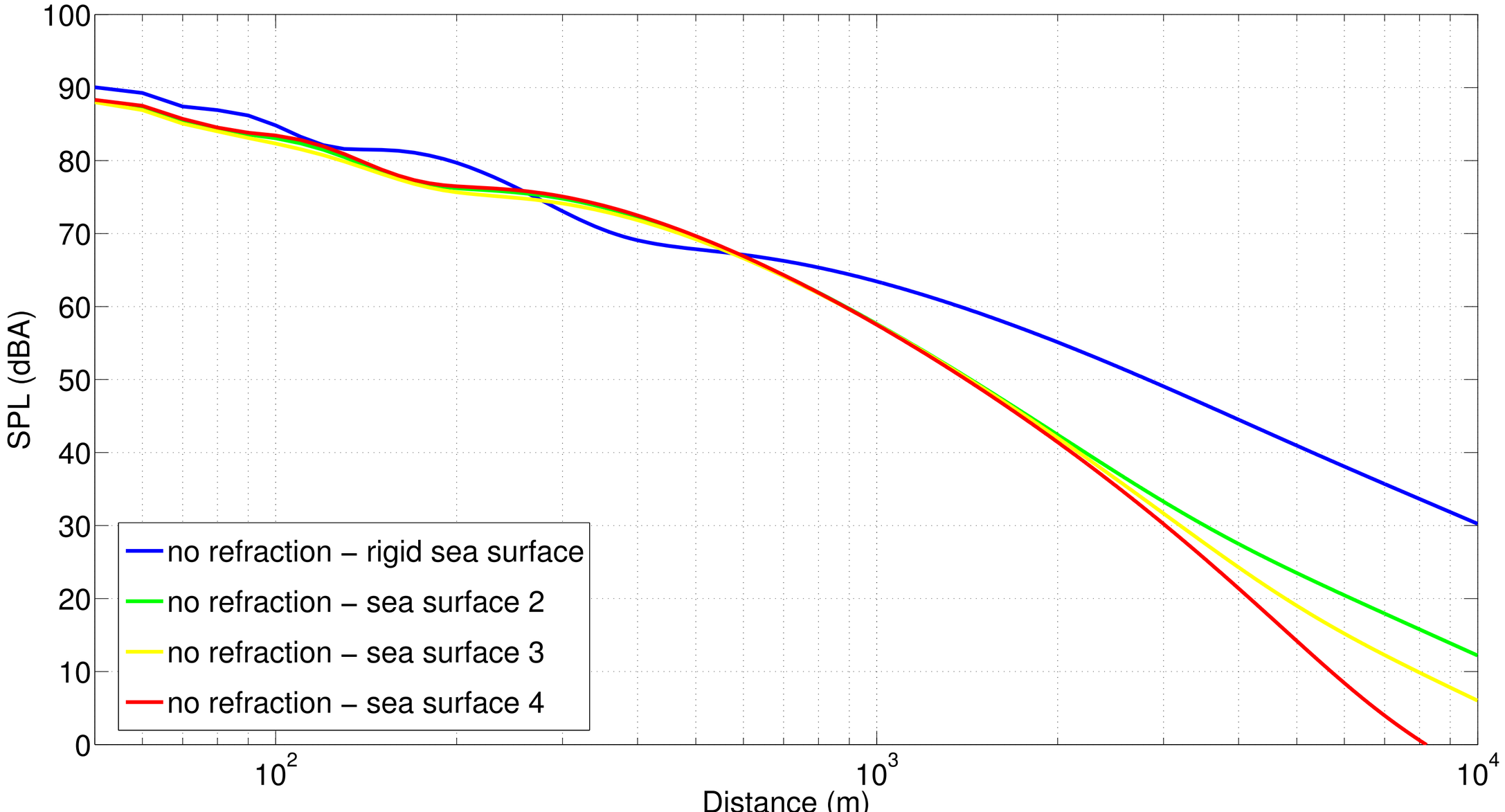
100
90
80
70
60
50
40
30
20
10
0
SPL (dBA)
10^2
10^3
10^4
Distance (m)
no refraction – rigid sea surface
no refraction – sea surface 2
no refraction – sea surface 3
no refraction – sea surface 4

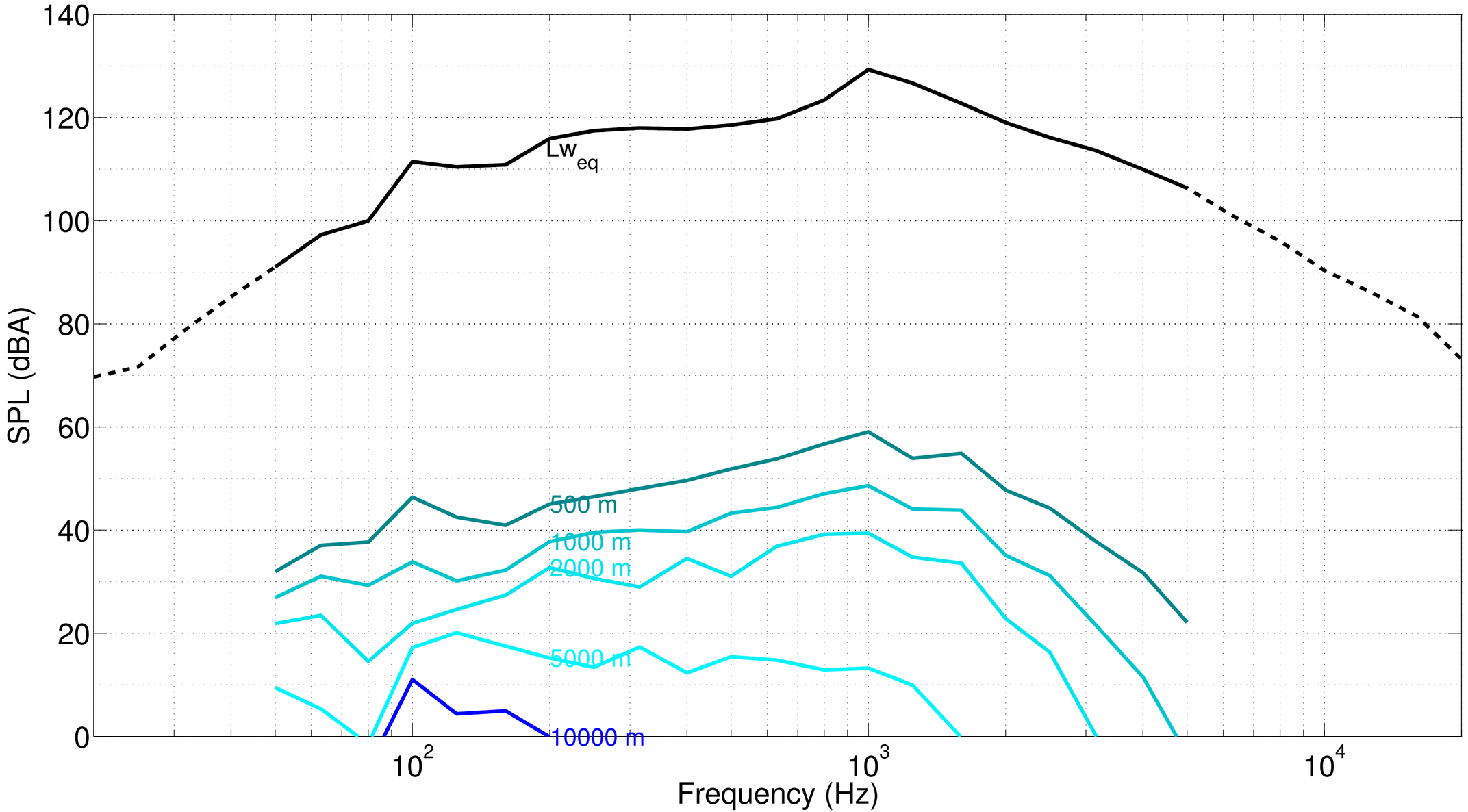
140
120
100
80
60
40
20
0
SPL (dBA)
Lw
eq
500 m
1000 m
2000 m
5000 m
10000 m
10^2
10^3
10^4
Frequency (Hz)